Int. J. Electrochem. Sci., 12 **(2017)** 1929 – 1942, doi: 10.20964/2017.03.33

International Journal of
ELECTROCHEMICAL
SCIENCE
www.electrochemsci.org

TiO_2/Sunflower Seed Shell-derived Carbon Micro Fiber Hybrids as Promising Anode Materials for Sodium-ion Batteries

Yang Zhao[1], *Shou-Dong Xu*[1,2,*], *Ding Zhang*[1,2], *Shibin Liu*[1], *Liang Chen*[1], *Hanqing Zhao*[2], *Guoqiang Wei*[1,2,*]

[1] College of Chemistry and Chemical Engineering, Taiyuan University of Technology, Taiyuan, 030024, P. R. China
[2] Lab of Green Energy Materials and Storage Systems, Taiyuan University of Technology, Taiyuan, 030024, P. R. China
[*]E-mail: xushoudong@tyut.edu.cn, weiguoqiang@tyut.edu.cn

Received: 10 December 2016 / *Accepted:* 13 January 2017 / *Published:* 12 February 2017

TiO_2/sunflower seed shell-derived carbon micro fiber hybrids have been synthesized via a facile hydrothermal method followed by annealing process. The resulting structure does not vary after carbon micro fibers (CMFs) introduced. The composites consist of CMFs with a diameter of about 4 μm and some TiO_2 nanoparticles attached on the surface of CMFs. The obtained material has been used as anode for sodium-ion battery. The results of the electrochemical tests showed that TiO_2/CMFs electrode delivered a superior reversible capacity of 214 mAh g^{-1} after 100 cycles at 30 mA g^{-1}, which is a dramatic improvement compared with commercial TiO_2 electrode. Remarkably, TiO_2/CMFs electrode still showed an excellent long-term cycling after 500 cycles at 500 mA g^{-1}. The good electrochemical properties of TiO_2/CMFs hybrids can be ascribed to the addition of CMFs, which can not only offer the efficient pathway for ion diffusion and electron transportation, but also provide an excellent contacting with the current collector.

Keywords: Sodium-ion battery, Carbon micro fiber, TiO_2, Sunflower seed shell, Anode

1. INTRODUCTION

Ever-growing energy needs and depleting fossil-fuel resources demand the pursuit of sustainable energy alternatives, including both renewable energy sources and sustainable storage technologies [1]. Lithium-ion batteries (LIBs) have emerged as one of the most popular choice for energy storage in portable devices, since their early commercialization in the 1990s. The success of LIBs has been mainly attributed to their high energy density, long cycle life and affordable cost [2]. However, the large-scale demand for lithium would require us to consider the growing price of lithium

resources because of the low abundance of Li element in the Earth's crust [3]. The limitation of lithium resources and the rising cost create a barrier for using LIBs in large-scale storage applications. Unlike lithium, sodium is one of the most abundant resources in sea water and salt deposits [4, 5]. On the other hand, sodium is the second lightest and smallest alkali metal next to lithium, and in fact the chemistry properties of Li and Na are similar in general, that could make sodium-based batteries especially sodium-ion batteries (SIBs) providing an alternative chemistry to LIBs.

Recently, a huge variety of suitable cathode materials for SIBs have already been identified and developed, including layered oxide compounds [6-8], polyanionic compounds [9-11] and Prussian blue analogues [12-14]. However, with respect to the anode materials, there were only few materials reported so far. Graphite, as predominantly anode material for commercial LIBs, has been proven to have negligible intercalation capacity as an anode for SIBs [15, 16]. Disordered carbons, especially for hard carbons, exhibit high Na^+ intercalation capacity and emerges as a leading candidate for SIBs applications. Nevertheless, low operational potential raises severe safety issues for practical applications, as for instance, metallic sodium plating and sodium dendrite formation. On the other hand, previous findings have demonstrated that alloy-type (Sn [17, 18], Ge [19], Si [20] and P [21, 22]) anode materials exhibited high initial capacity, but suffered from poor cyclability most likely due to the large volume changes during cycling. The huge volume changes of these materials can cause the pulverization of the electrode, eventually leading to battery failure.

Among all the anode materials that have been reported for SIBs, titanium dioxide (TiO_2) with the merits of exceptional chemical stability, nontoxicity, low-cost and elemental abundance, has been regarded as a promising one for SIBs [23]. Up to now, several types of TiO_2 such as amorphous TiO_2 [24], TiO_2 nanorods [25], TiO_2 microsphere [26], anatase TiO_2 nanoparticles [27] and TiO_2 (B) nanotubes [28] have been intensively studied as anode materials in SIBs. However, the main problem of TiO_2 is its low electrical conductivity (only about 1×10^{-12} to 1×10^{-7} S cm^{-1} [29]) owing to its high band gap of 3.2 eV, which gives rise to the insulating nature of intrinsic TiO_2 without a dopant [30]. In order to improve the electrochemical properties especially reversible capacity of TiO_2 at high current destiny, two main strategies have been proposed to increase the electron or ions transport rate of TiO_2. One general method is to achieve nanostructural TiO_2 with larger surface areas, resulting in higher reversible capacity, better cyclability and rate performance. Another effective way is to design TiO_2 with advanced carbonaceous materials, namely preparing TiO_2/carbon composites, such as TiO_2/C [31, 32], TiO_2/carbon nanotubes [33] and TiO_2/graphene [34-36]. Although the strategy of fabricating TiO_2/carbon composite has resulted enhanced electrochemical performances, the manufacturing process is complex and the fabricating cost is expensive, thus raising concerns about the availability and large scale productions of TiO_2/C. Therefore, searching for a simple and cost effective method for designing TiO_2/C anode materials for SIBs that can possess excellent electrochemical performance particularly long term cyclability and high rate charge-discharge performance is extremely urgent.

A simple, cost effective, and economical route for preparation of carbon materials is biomass or biomass waste derived technology. Recently, hard carbons and porous hard carbons have received a tremendous amount of attentions in a variety of fields, especially in energy storage. Hard carbons derived from biomass or biomass waste have been widely investigated for electrochemical electrode materials, such as nanostructured silicon from rice husks for high-performance LIBs anode materials

[37], litchi shells-derived activated carbon for Li-S batteries [38], and peanut shell hybrid for Na-ion capacitor [39]. In addition, hard carbons have been applied to prepare the composite of transition metal oxide with carbon, owing to its good conductivity and abundant sources [40].

Sunflower (Helianthus annuus) seeds, as an important kind of agricultural crops, can be transformed to sunflower oil. There is plenty of sunflower seed shell produced as biowaste from sunflower seed processing every year. Actually, the sunflower seed shell has a particular with bulky directional arrangement of carbon fibers. If we can use an effective method to dissolve the lignin part which often plays an important role in binding carbon fibers together and make the individual carbon fibers extracting from the bulky carbons, the sunflower seed shell should be fully utilized.

Herein, in this work, we demonstrate a simple and green route to form TiO_2/sunflower seed shells derive carbon micro fibers hybrid composites. The structure and morphology were characterized, and the sodium storage properties of TiO_2/carbon micro fibers were investigated in coin cells. The TiO_2/carbon micro fibers electrodes exhibit high reversible capacity, stable Coulombic efficiency, superior rate performance and excellent long-term cycling performance compared to the TiO_2 electrode. The good electrochemical properties of TiO_2/CMFs hybrids can be ascribed to the addition of CMFs, which can not only offer the efficient pathway for ion diffusion and electron transportation, but also provide an excellent contacting with the current collector.

2. EXPERIMENTAL

2.1 Synthesis of carbon micro fibers

Sunflower seeds were used here as raw materials and purchased from the local market. Firstly, sunflower seed shells were peeled off from the seeds, washed with distilled water and ethanol by ultrasonic cleaning, then they were dried in an electric oven at 90 ℃ for 12 hours. Within the underlying hydrothermal treatment, 2 g of the dried sunflower seed shells were put into a 100 mL Teflon-lined stainless steel autoclave, and then 80 mL of homogeneous 3 M NaOH solution was added into the above Teflon tank. After that, the autoclave was sealed and placed still in an electric oven at 165 ℃ for 6 h. Then, the samples were collected by vacuum filtration and washed by 0.1 M HCl and distilled water several times until the pH valve of the solution reached above 6, and then dried at 90 ℃ for 12 h. After the drying process, the yellowish-white and fluffy carbon micro fibers (termed: uncarbonized CMFs) were obtained. To get carbonized carbon micro fibers (termed: CMFs), the uncarbonized CMFs were transferred to a tube furnace and calcined at 800℃ with a heating rate of 5℃ min^{-1} for 2 h under Ar atmosphere.

2.2 Synthesis of TiO_2/CMFs hybrids

The uncarbonized CMFs and commercial TiO_2 powders (Sigma-Aldrich Company) were used as raw materials. Typical synthesis can be described as follows. Firstly, NaOH and TiO_2 powders with a molar ratio of 2:3 were dissolved in distilled water and stirred with a magnetic stirring for 2 h. Then,

uncarbonized CMFs were immersed into the solution and continued to stir for 2 h to form a uniform solution. Next, 80 mL of the uniform solution was put into a 100 mL Teflon-lined stainless steel autoclave, and the autoclave was sealed and kept in an electric oven at 150 ℃ for 12h. The products were washed and centrifuged with distilled water and dried at 90 ℃ for 12 h. Last, the samples were calcined in a tube furnace at 750 ℃ for 5 h (a heating rate of 10 ℃ min^{-1}) under argon flow of 100 mL min^{-1}. After that, TiO_2/CMFs hybrids were obtained eventually.

2.3 Materials characterization

Thermogravimetric analysis (TGA) was carried out on a thermal analysis instrument (Netzsch STA 449 F3) with a heating rate of 10 ℃ min^{-1} (from room temperature to 1000℃) in N_2 atmosphere. The structures of the samples were investigated by X-ray diffractometer (XRD) (Philips, Netherlands) with Cu-Kα radiation within the 2θ range of 10-80° and Raman spectroscopy (Bruker VERTEX 70, USA). The morphologies of the samples were investigated by field-emission scanning electron microscopy (FESEM, MIRA3, TESCAN).

2.4 Electrochemical measurements

Electrochemical tests were performed with CR2025 type coin cell. Assembling of the coin cells was operated in an argon-filled glove box (Mbraun, Germany). Firstly, the working electrode was prepared by mixing the active materials, Super P and polyvinylidene fluoride (PVDF) binder in a weight ratio of 8:1:1 dissolved in N-methyl-2pyrrolidinine (NMP) solvent. After stirring for 2h, the slurry was uniformly pasted onto copper foil, and then the electrodes were dried in an oven at 80 ℃ for 12h. After that, the electrodes were transferred to the glove box with the concentrations of moisture and oxygen less than 0.5 ppm. Sodium foil was used as the counter electrode. The electrolyte was 1M $NaClO_4$ dissolved in ethylene carbonate (EC) and propylene carbonate (PC) in a volume ratio of 1:1. Glass fiber membrane (Whatman) was used as the separator. The coin cells were galvanostatically charged and discharged in a battery analyzers (LAND, Wuhan, China) over a range of 2.0-0.001 V vs. Na/Na^+ at different constant current density. Cyclic voltammetry (CV) tests were performed on an electrochemical workstation (CHI660E) at a scan rate of 0.1mV s^{-1}. Electrochemical impedance spectroscopy (EIS) analyses were conducted with an applied initial voltage of 5 mV in the range of 100 kHz to 0.01 Hz. All the electrochemical tests were carried out at room temperature.

3. RESULTS AND DISCUSSION

3.1 Structural and morphological characterization

To evaluate the content of TiO_2 in the hybrids and to understand the thermal decomposition behaviors of uncarbonized CMFs, thermogravimetric analysis was introduced. TGA curves of TiO_2 powders, TiO_2/CMFs precursor and uncarbonized CMFs were presented in Fig. 1. The TGA curve of

the TiO_2 powders in the whole temperature range tends to be a straight line, with only the mass loss of 1.61%, indicating that there is no phase change for the pure TiO_2 powders. On the other hand, for uncarbonized CMFs and TiO_2/CMFs precursor, the mainly weight loss occured at 300 to 400 ℃, which can be attributed to the pyrolysis of lignin, cellulose and hemicellulose in the biomass. It also can be seen that there is no obvious mass loss when the temperature is higher than 600 ℃, and TGA curves for all the samples tend to flatten. Based on above, the content of TiO_2 in the TiO_2/CMFs hybrids is calculated to be about 52%.

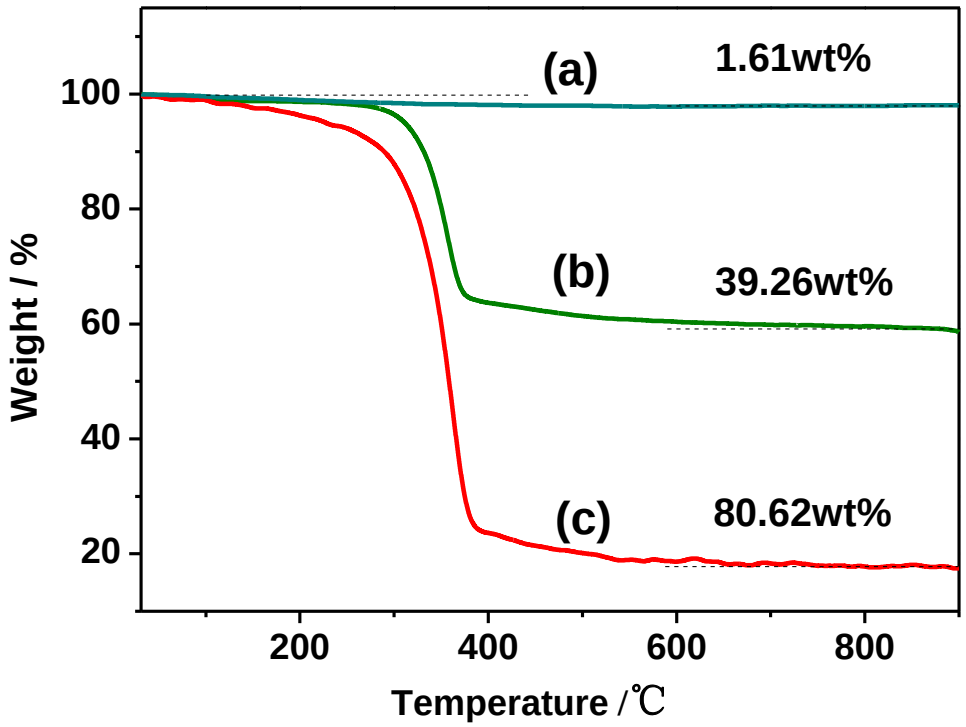

Figure 1. TGA curves of (a) TiO_2 powders, (b) TiO_2/CMFs precursor and (c) uncarbonized CMFs.

The XRD patterns of CMFs, commercial TiO_2 powders and TiO_2/CMFs hybrids are shown in Fig. 2. For CMFs, shown in Fig. 2(a), there are only two broad peaks at about 23° and 43°, which correspond to the (002) and (100) planes of graphite, respectively. The broad and weak peaks also indicate that CMFs are typical of hard carbon materials with disordered nanocrystalline structure [41]. The XRD patterns of TiO_2 and TiO_2/CMFs are shown in Fig. 2(b). The major diffraction peaks of both samples at 25.3°, 37.8°, 48.0°, 53.9°, 55.1°, 62.7° and 75.0° indicate the (101), (004), (200), (105), (211), (204) and (215) planes of anatase TiO_2 (JCPDS No. 21-1272), respectively, which has the tetragonal space group with $I4_1/amd$ [27, 42]. Moreover, since CMFs in the TiO_2/CMFs hybrids are amorphous, no obvious carbon peaks are observed in the XRD pattern in Fig. 2(b). Meanwhile, it also can be seen that the addition of CMFs did not impact the crystal structure of TiO_2.

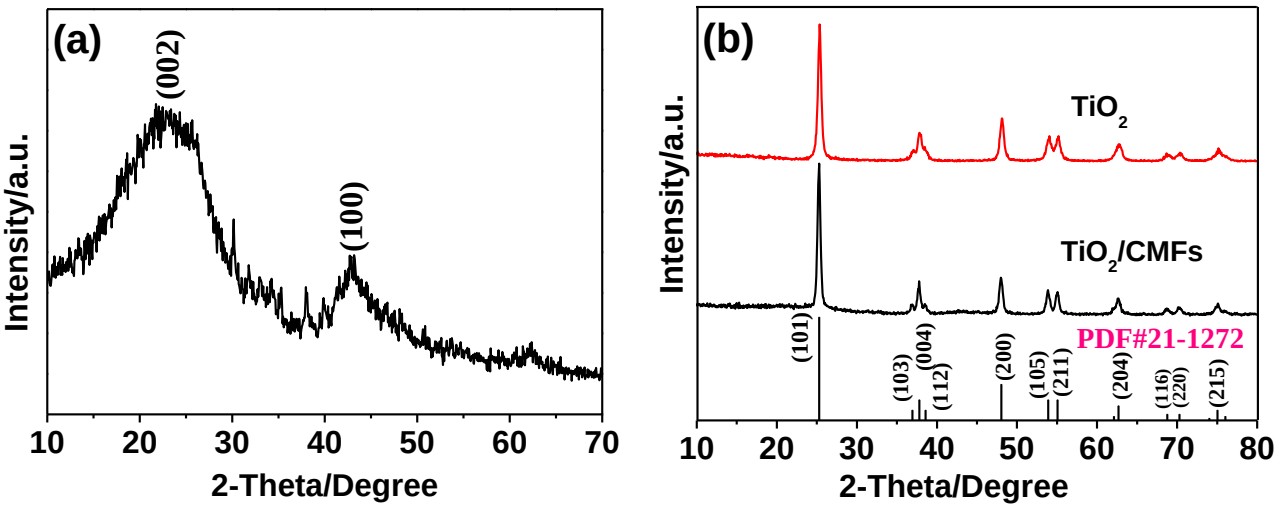

Figure 2. XRD patterns of (a) CMFs and (b) TiO_2 powders and TiO_2/CMFs hybrids; the reference for anatase TiO_2 (JCPDS card No. 21-1272) is shown in the bottom.

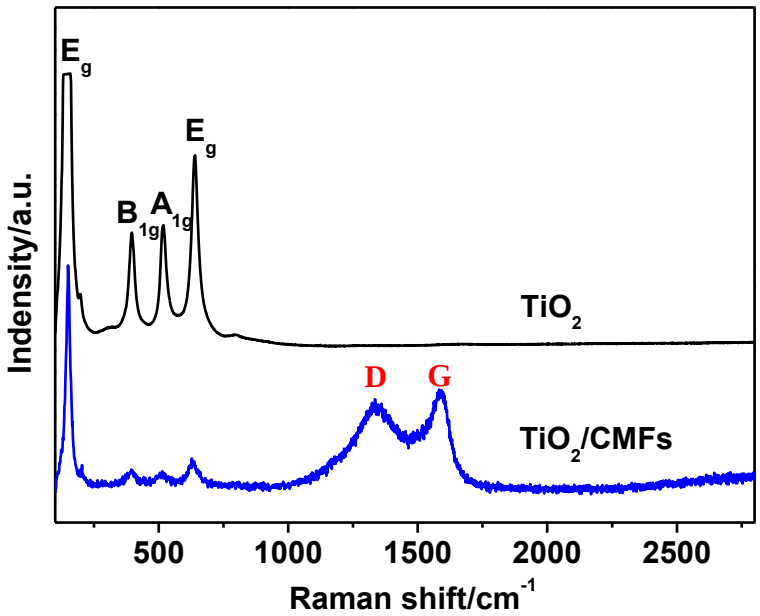

Figure 3. Raman spectra of TiO_2 powders and TiO_2/CMFs hybrids.

Raman spectra were used to further identify the structure of the hybrids, as shown in Fig. 3. The Raman spectra of TiO_2 particles exhibit four separated peaks located at around 145, 397, 515 and 639 cm^{-1} which can be assigned to the E_g, B_{1g}, B_{1g} or A_{1g} and E_g modes of anatase phase [35, 43]. No other Raman peaks can be observed, which means that the TiO_2 particles are pure anatase. On the other hand, Raman spectra of TiO_2/CMFs hybrids also contain the E_g, B_{1g}, B_{1g} or A_{1g} and E_g bands of the anatase TiO_2, which also confirms that introduced CMFs cannot change the structure of the samples. Such a conclusion is consistent with the XRD result shown in Fig. 2. Moreover, Raman spectra of TiO_2/CMFs hybrids exhibit two characteristic bands around 1343 cm^{-1} (D-band) and 1591 cm^{-1} (G-

band), corresponding to a defect-induced mode and the E_{2g} graphitic model [44]. The Raman analysis is clearly verified that the structural properties of the hybrids did not change after CMFs were used.

Fig. 4 (a) and (b) show the morphology of TiO_2/CMFs hybrids, and the inset in Fig. 4 (b) is the SEM image of an individual carbon fiber derived from sunflower seed shell with a diameter of about 4 μm long. For the TiO_2/CMFs hybrids, it can be seen that some TiO_2 particles aggregated with part of carbon fibers crossing on the composites. Obviously, there are also some TiO_2 particles anchored on the wrinkled surface of carbon fibers. Moreover, to further definition of the elements distribution, the EDS analysis of TiO_2/CMF was carried out. Fig. 4 (c)-(e) show the corresponding elemental mapping of carbon, oxygen and titanium. As it can be seen, titanium and oxygen elements repeat the existence of carbon elements, suggesting the dispersion of TiO_2 on the surface of CMFs.

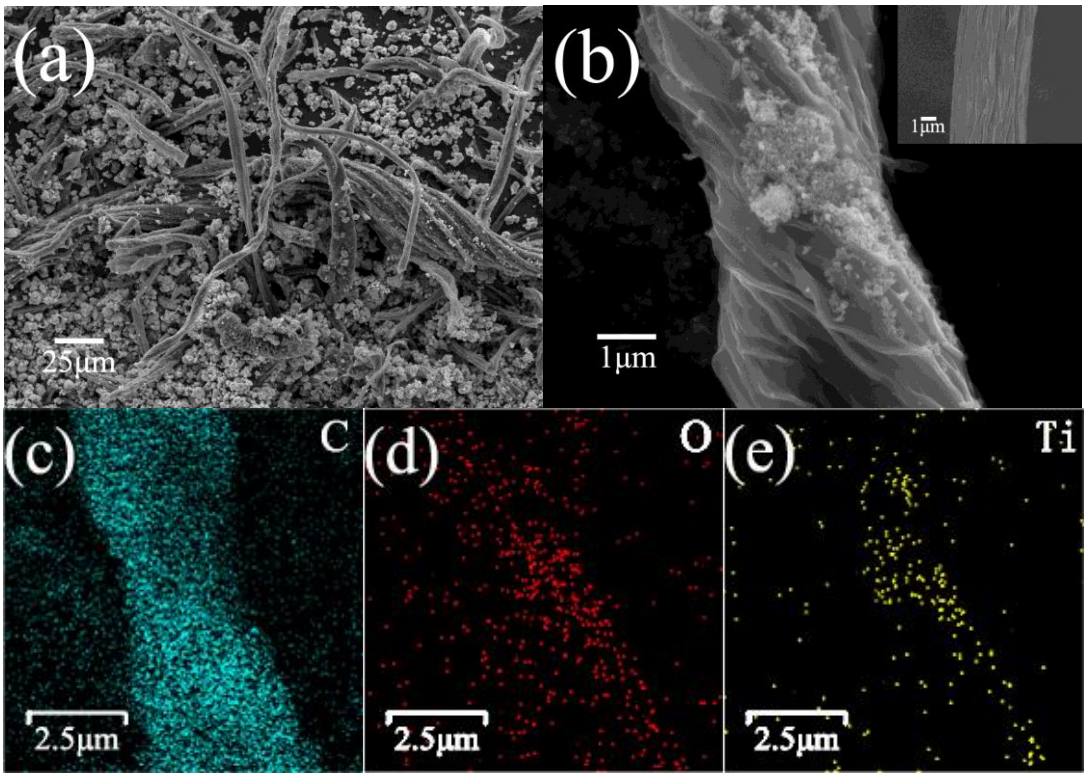

Figure 4. SEM images of (a, b) TiO_2/CMFs hybrids; EDS map of (c) carbon element, (d) oxygen element and (e) titanium element. The inset in Fig. 4 (b) is the SEM image of CMFs.

3.2 Electrochemical performance

Fig. 5 exhibit the cyclic voltammetry (CV) curves of TiO_2 and TiO_2/CMFs electrodes at a scan rate of 0.1 mV s^{-1}. For TiO_2 electrode, the first cathodic peak at about 0.42V in the first cycle was assigned to the formation of solid electrolyte interface (SEI) film, which was the same as the irreversible peak of TiO_2/CMFs electrode at approximately 0.35V. The cathodic peak near reversing potential of 0.001V can be attributed to the processes of sodiation and electrolyte decomposition [35]. With subsequent cyclic sweeps, for both TiO_2 and TiO_2/CMFs electrodes, there was a pair of redox

peaks responding to redox couple of Ti^{4+}/Ti^{3+} [35]. In addition, an intense anodic peak of TiO_2 (Fig. 5 (a)) from 2nd to 5th cycle at around 0.09V was possibly related to the reversible sodium release [27]. Meanwhile, a slighter anodic peak of TiO_2/CMFs (Fig. 5(b)) was obversed at about 0.15V, which might be caused by the reversible sodium release as TiO_2, presumably resulted from TiO_2 and shifted to higher potential. It is worth noting that the subsequent cyclic sweeps of TiO_2/CMFs electrode have a better coincidence than that TiO_2 electrode, revealing that TiO_2/CMFs hybrids can present better electrochemical properties, especially in terms of reversibility.

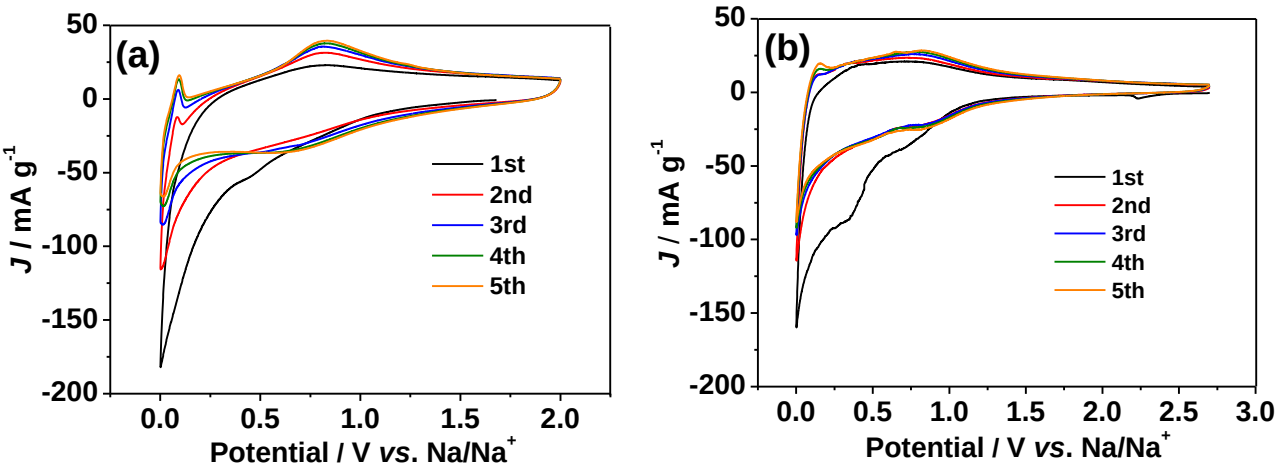

Figure 5. Cyclic voltammetry curves of (a) TiO_2 powders and (b) TiO_2/CMFs hybrids at a scan rate of 0.1 mV s^{-1}.

To further understand the electrochemical properties of TiO_2/CMFs hybrids, galvanostatic charge-discharge technology was performed. Fig. 6 (a)-(c) show the charge-discharge profiles of TiO_2, CMFs and TiO_2/CMFs hybrids electrodes at a current density of 30 mA g^{-1}. The potential profiles for the commercial TiO_2 electrode are sloping curves, delivering a reversible capacity of approximately 120.6 mAh g^{-1}. Importantly, a short plateau voltage appeared below 0.1 V for CMFs and TiO_2/CMFs hybrids electrodes, which probably represent the Na^+ insertion and extraction in the hard carbon matrix. In addition, compared with the first cycle, the charge capacity of the second and third cycle for TiO_2 electrode was decreased, whereas CMFs and TiO_2/CMFs hybrids electrodes were increased. The cycle performances of the above electrodes are shown in Fig. 6(d). The stable charge capacities of TiO_2, CMFs and TiO_2/CMFs were about 121, 188 and 214 mAh g^{-1} after 100 charge-discharge cycles. It was noteworthy that adding of CMFs in the hybrids can reduce the undulation of the cycling capacity.

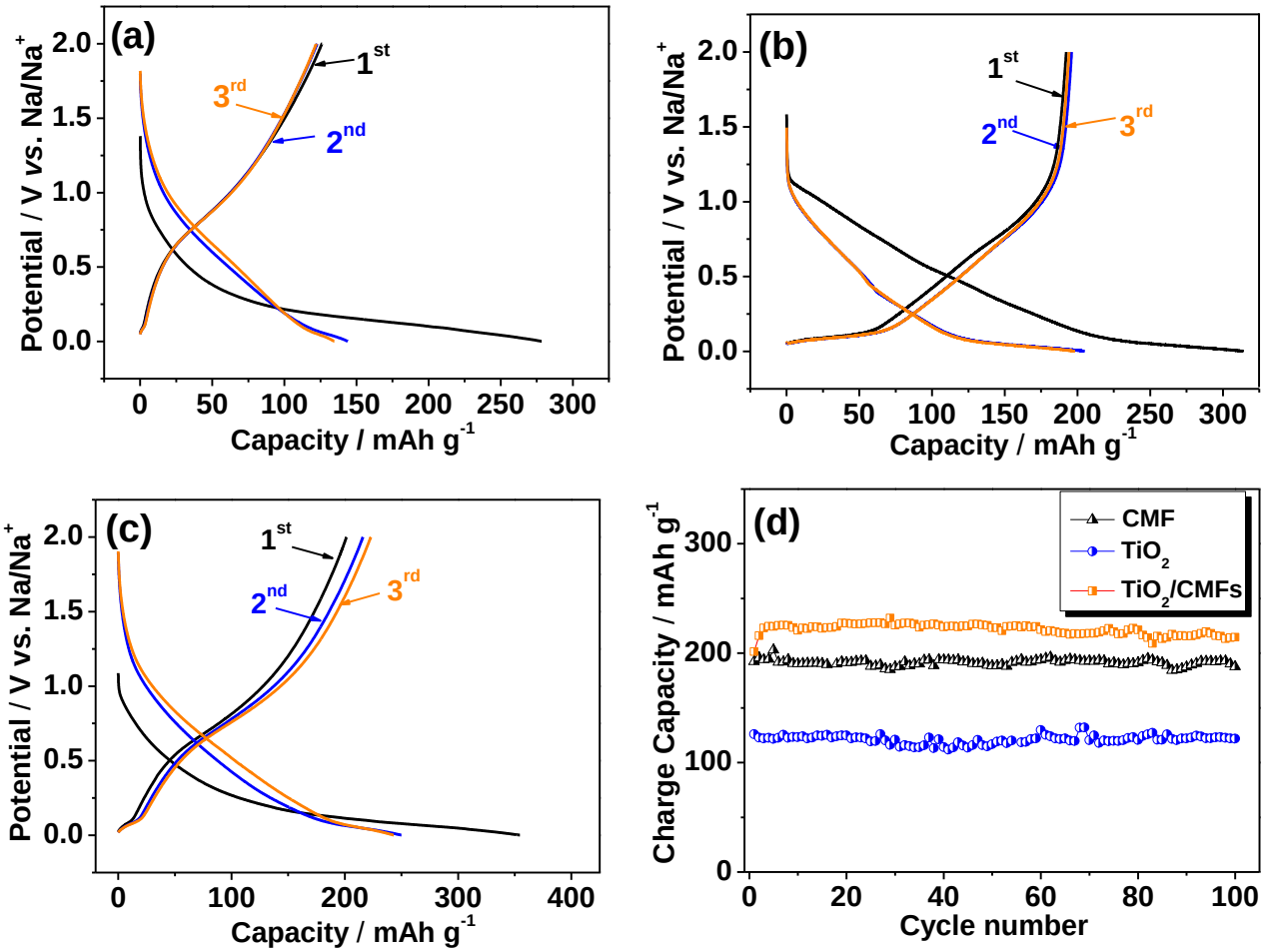

Figure 6. Charge and discharge curves of (a) TiO_2 powders, (b) CMFs and (c) TiO_2/CMFs hybrids at 30 mA g^{-1}. (d) Cycling performance of TiO_2 powders, CMFs and TiO_2/CMFs hybrids at 30 mA g^{-1} for 100 cycles.

Table 1. Comparison of the electrochemical performance of TiO_2 electrodes recently reported in the literature with the TiO_2/CMFs electrode presented in this work.

Sample	Capacity/ (mAh g^{-1})	Cycling capacity retention	Initial Coulombic efficiency	Reference
Anatase TiO_2 nanocrystals	150 at 50 mA g^{-1} after 100 cycles	70.8%	41.9%	[23]
Carbon-coated-nanorod TiO_2	178 at 10 mA g^{-1} after 100 cycles	92.2%	<30%	[25]
Carbon-coated TiO_2 microsphere	155 at 0.1C after 50 cycles	--	45.8%	[26]
Anatase TiO_2 nanoparticles	135 at 36.9 mA g^{-1} after 60 cycles	93.1%	46.4%	[27]
Carbon-coated TiO_2 nanoparticles	210.7 at 30 mA g^{-1} after 100 cycles	87.0%	57.1%	[31]
Nanocrystalline anatase TiO_2–graphene composite	143 at 36.9 mA g^{-1} after 50 cycles	91.7%	60.0%	[36]
TiO_2/carbon hollow spheres	140.4 at 100 mA g^{-1} after 100 cycles	91.1%	25.7%	[45]

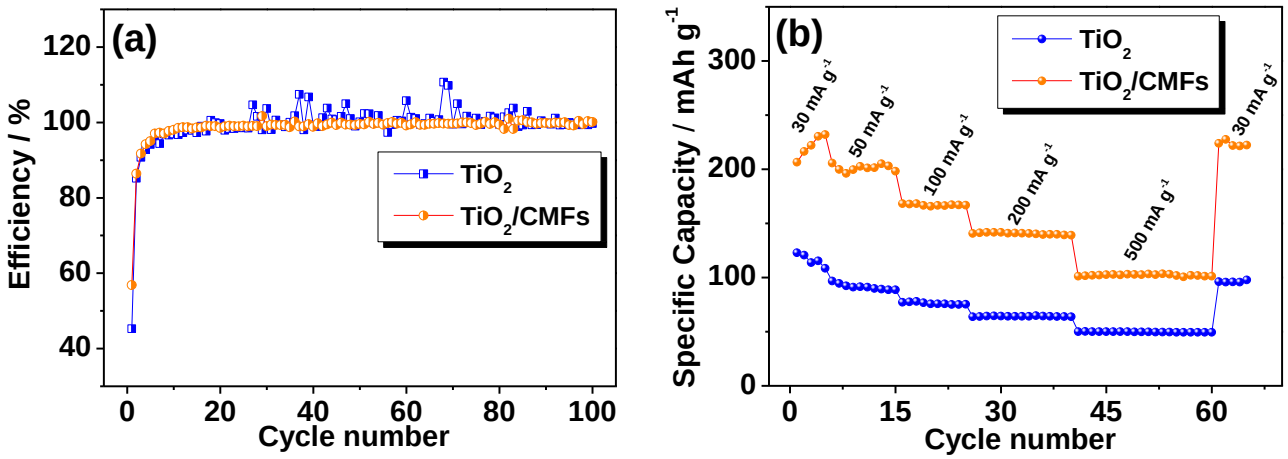

Figure 7. Effect of cycling on (a) Coulombic efficiencies and (b) rate performance of TiO_2 powders and TiO_2/CMFs hybrids.

It must also be mentioned that the initial Coulombic efficiency and the stability of the Coulombic efficiency during the subsequently cycles were both increased when the CMFs introduced, as seen in Fig. 7(a). In comparison, the initial Coulombic efficiencies of TiO_2 and TiO_2/CMFs electrodes were 45.3% and 56.8%, respectively, which were higher than other reported anatase TiO_2 material [45]. After the first cycle, the Coulombic efficiency of TiO_2/CMFs was increased to 86.3% in the second cycle, and then the latter exceeded over 97% after 5 cycles. Moreover, the electrochemical performance of TiO_2 electrodes recently reported in the literature was demonstrated in the Table 1.

Rate capabilities of TiO_2 and TiO_2/CMFs hybrids electrodes are illustrated in Fig. 7 (b). The reversible capacities of TiO_2 were 113.8, 91.5, 75.8, 64.2 and 49.8 mAh g^{-1} at a series current densities of 30, 50, 100, 200 and 500 mA g^{-1}, while for the TiO_2/CMFs hybrids electrode, the reversible capacities can reach to 222.1, 202.6, 166.7, 141.1 and 103.2 mAh g^{-1} at the same series of current densities. Comparing with the initial capacity at 30 mA g^{-1}, the capacity retention of TiO_2/CMFs was over 99% when the current density was reversed back to 30 mA g^{-1}, while the capacity retention of TiO_2 was only 78.7% under the same condition. In comparison, rate capabilities of TiO_2/CMFs assumed a more obvious improvement at all current densities and the good rate performance was presented.

Fig. 8 shows the long-term cycling performance of TiO_2/CMFs electrode at 30 mA g^{-1} for the first 5 cycles and 500 mA g^{-1} for 500 cycles. The reversible capacity of TiO_2/CMFs was about 216 mAh g^{-1} after the battery activation process at the low current density of 30 mA g^{-1}. And then the current density was increased to 500 mA g^{-1} (equivalent to 2C rate), the capacity was still stable at 104 mAh g^{-1} after 500 cycles with the capacity retention of 94.1%. Indeed, the Coulombic efficiency of TiO_2/CMFs at 500 mA g^{-1} was stable at around 100% after 10 cycles, which also indicated the stable long-term cycling performance of TiO_2/CMF.

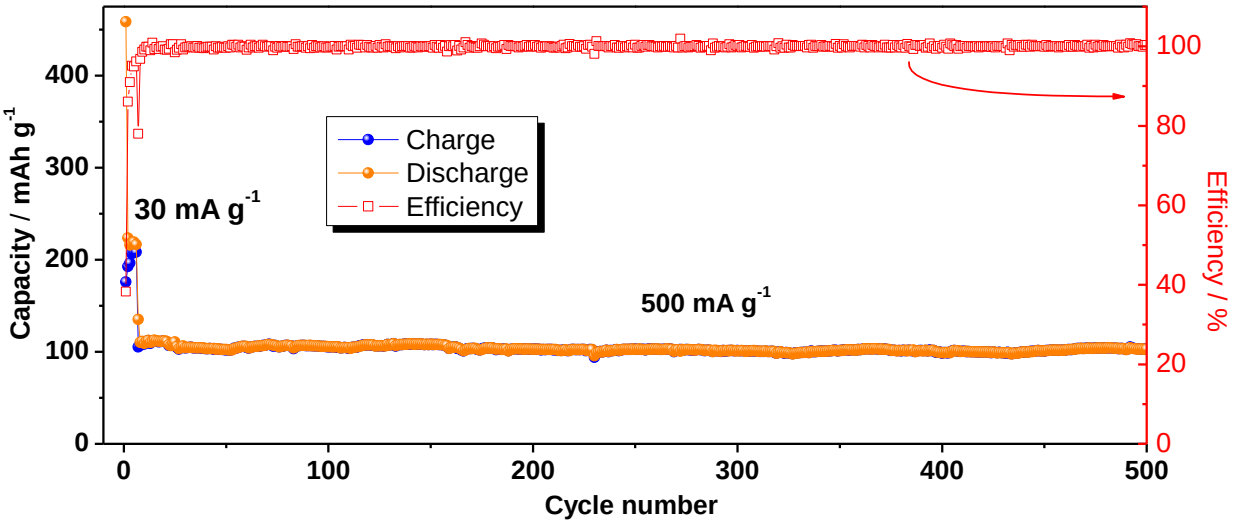

Figure 8. Long-term cycling performance and Coulombic efficiency of TiO_2/CMFs hybrids electrode at 30 mA g^{-1} for the first 5 cycles and 500 mA g^{-1} for 500 cycles.

EIS is one of the most important and useful techniques that can provide unique information about the nature of the electrode during the polarization processes [47, 48]. Fig. 9 shows the Nyquist plots of TiO_2 and TiO_2/CMF electrodes at 0.1 V in the discharge process. For both electrodes, it can be seen that the Nyquist plots include a depressed semicircle in the high-middle frequency region which is attributed to the charge transfer process and a straight line related to the Warburg diffusion process in the low-frequency region. It can be obvious seen that the diameter of the charge transfer semicircle for TiO_2/CMFs electrode is much smaller than that of TiO_2 electrode, indicating that TiO_2/CMFs materials have the lower charge transfer resistance than TiO_2, resulting in more easily transportation of electrons and ions [40]. Hence, the TiO_2/CMFs electrode has a considerable improvement of capacity and charge transfer conductivity.

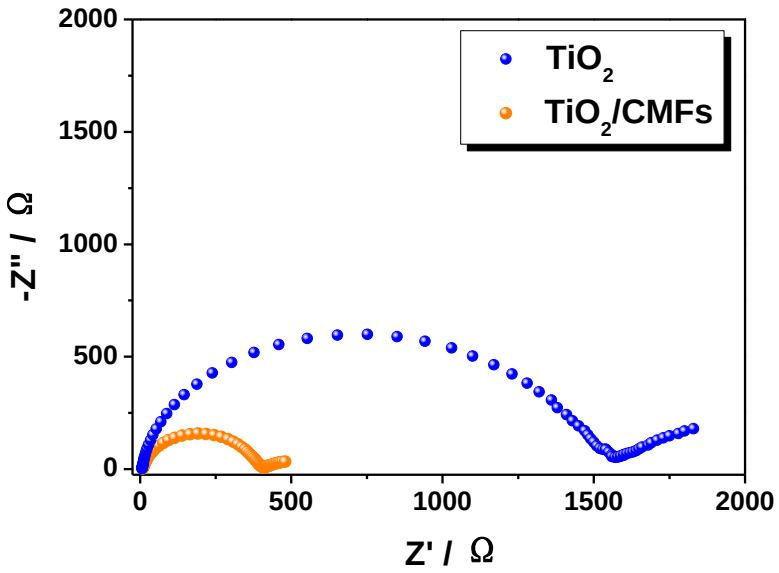

Figure 9. Nyquist plots of TiO_2 and TiO_2/CMFs electrodes.

Sunflower seed shells-derived CMFs in the hybrids play an important role in improving the electrochemical properties of TiO_2/CMFs. The schematic illustration of the ions and electrons transport mechanism for TiO_2/CMFs hybrids is shown in Fig. 10. On the one hand, CMFs can provide extra capacity of Na^+ storage. On the other hand, the fibrous structure not only offering the efficient pathway to the transport of Na^+ and e^-, but also providing a good electron conducting network and an excellent contacting with the current collector. Thus, the superior reversible capacity and a better rate capability for the TiO_2/CMFs electrode can be obtained.

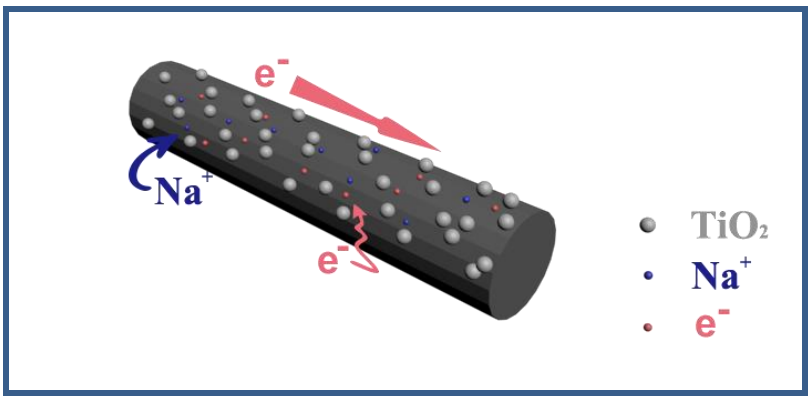

Figure 10. Schematic illustration of the ions and electrons transport mechanism for TiO_2/CMFs hybrids in SIBs.

4. CONCLUSIONS

In summary, TiO_2/sunflower seed shell-derived carbon micro fiber hybrids have been successfully prepared through a facile hydrothermal method followed by annealing at 750℃ for 5 h in Ar atmospheres. XRD and Raman techniques confirm that the introduction of carbon micro fibers can not change and has no impact on the crystal structure of anatase TiO_2. SEM images show that the carbon micro fibers cross the whole hybrid composites and some TiO_2 nanoparticles are attached on the surface of CMFs. When being applied as an anode material for sodium-ion battery, the TiO_2/CMFs electrode can deliver a superior reversible capacity of 214 mAh g^{-1} after 100 cycles at 30 mA g^{-1}, which is a dramatic improvement compared with the commercial TiO_2 powders electrode. More importantly, the TiO_2/CMFs electrode can show a noticeable improvement in rate performance and long-term cycling, which can achieve a stable capacity up to 500 cycles at 500 mA g^{-1}. The good cyclability and a high-rate capability of the hybrids indicate that the TiO_2/CMFs are proposed to be applied as next generation high-performance electrode materials for rechargeable sodium-ion batteries. Also, this work can provide a simple and green route to form TiO_2/biomass-derived carbon materials that could possess satisfactory micro-nano structure and excellent electrochemical performance.

ACKNOWLEDGMENT
This work was supported by the National Natural Science Foundation of China (Grant No. 21506141, 21606158) and Natural Science Foundation of Shanxi Province (Grant No. 2015021131).

References

1. D. Larcher, J.M. Tarascon, *Nat. Chem.*, 7 (2015) 19.
2. L.P. Wang, L. Yu, X. Wang, M. Srinivasan, Z.J. Xu, *J. Mater. Chem. A*, 3 (2015) 9353.
3. H.-G. Wang, S. Yuan, D.-L. Ma, X.-B. Zhang, J.-M. Yan, *Energy Environ. Sci.*, 8 (2015) 1660.
4. N. Yabuuchi, M. Yano, H. Yoshida, S. Kuze, S. Komaba, *J. Electrochem. Soc.*, 160 (2013) A3131.
5. M. Dahbi, N. Yabuuchi, K. Kubota, K. Tokiwa, S. Komaba, *Phys. Chem. Chem. Phys*., 16 (2014) 15007.
6. D.J. Kim, R. Ponraj, A.G. Kannan, H.-W. Lee, R. Fathi, R. Ruffo, C.M. Mari, D.K. Kim, *J. Power Sources*, 244 (2013) 758.
7. J. Billaud, R.J. Clement, A.R. Armstrong, J. Canales-Vazquez, P. Rozier, C.P. Grey, P.G. Bruce, *J. Am. Chem. Soc*., 136 (2014) 17243.
8. N. Yabuuchi, M. Kajiyama, J. Iwatate, H. Nishikawa, S. Hitomi, R. Okuyama, R. Usui, Y. Yamada, S. Komaba, *Nat. Mater*., 11 (2012) 512.
9. S.-M. Oh, S.-T. Myung, J. Hassoun, B. Scrosati, Y.-K. Sun, *Electrochem. Commun*., 22 (2012) 149.
10. P. Barpanda, T. Ye, M. Avdeev, S.-C. Chung, A. Yamada, *J. Mater. Chem. A*, 1 (2013) 4194.
11. Y. Lu, S. Zhang, Y. Li, L. Xue, G. Xu, X. Zhang, *J. Power Sources*, 247 (2014) 770.
12. J. Qian, M. Zhou, Y. Cao, X. Ai, H. Yang, *Adv. Energy Mater*., 2 (2012) 410.
13. L. Wang, Y. Lu, J. Liu, M. Xu, J. Cheng, D. Zhang, J.B. Goodenough, *Angew. Chem., Int. Ed.*, 52 (2013) 1964.
14. Y. Lu, L. Wang, J. Cheng, J. B. Goodenough, *Chem. Commun.*, 48 (2012) 6544.
15. M.M. Doeff, Y.P. Ma, L.C. Dejonghe, *J. Electrochem. Soc.*, 140 (1993) L169.
16. P. Thomas, J. Ghanbaja, D. Billaud, *Electrochim. Acta*, 45 (1999) 423.
17. Y. Cheng, J. Huang, R. Li, Z. Xu, L. Cao, H. Ouyang, J. Li, H. Qi, C. Wang, *Electrochim. Acta*, 180 (2015) 227.
18. L. D. Ellis, T. D. Hatchard, M. N. Obrovac, *J. Electrochem. Soc.*, 159 (2012) A1801.
19. P.R. Abel, Y.-M. Lin, T. de Souza, C.-Y. Chou, A. Gupta, J.B. Goodenough, G.S. Hwang, A. Heller, C.B. Mullins, *J. Phys. Chem. C* ,117 (2013) 18885.
20. L.D. Ellis, B.N. Wilkes, T.D. Hatchard, M.N. Obrovac, *J. Electrochem. Soc*. 161 (2014) A416.
21. Y. Zh, Y. Wen, X. Fan, T. Gao, F. Han, C. Luo, S.-C. Liou, C. Wang, *ACS Nano*, 9 (2015) 3254.
22. L. Pei, Q. Zhao, C. Chen, J. Liang, J. Chen, *ChemElectroChem*, 2 (2015) 1652.
23. Y. Xu, E.M. Lotfabad, H. Wang, B. Farbod, Z. Xu, A. Kohandehghan, D. Mitlin, *Chem. Commun*., 49 (2013) 8973.
24. D. Su, S. Dou, G. Wang, *Chem. Mater.*, 27 (2015) 6022.
25. K.T. Kim, G. Ali, K.Y. Chung, C.S. Yoon, H. Yashiro, Y.K. Sun, J. Lu, K. Amine, S.T. Myung, *Nano Lett.*, 14 (2014) 416.
26. S.M. Oh, J.Y. Hwang, C.S. Yoon, J. Lu, K. Amine, I. Belharouak, Y.K. Sun, *ACS Appl. Mater. Interfaces*, 6 (2014) 11295.
27. L. Wu, D. Buchholz, D. Bresser, L. Gomes Chagas, S. Passerini, *J. Power Sources*, 251 (2014) 379.
28. J.P. Huang, D.D. Yuan, H.Z. Zhang, Y.L. Cao, G.R. Li, H.X. Yang, X.P. Gao, *RSC Advances*, 3 (2013) 12593.
29. W. Wang, Q. Sa, J. Chen, Y. Wang, H. Jung, Y. Yin, *ACS Appl. Mater. Interfaces*, 5 (2013) 6478.
30. D.A.H. Hanaor, C.C. Sorrell, *J. Mater. Sci.*, 46 (2011) 855.
31. Y. Ge, H. Jiang, J. Zhu, Y. Lu, C. Chen, Y. Hu, Y. Qiu, X. Zhang, *Electrochim. Acta*, 157 (2015) 142.
32. C. Ding, T. Nohira, R. Hagiwara, *J. Mater. Chem. A*, 3 (2015) 20767.
33. J.-Y. Hwang, S.-T. Myung, J.-H. Lee, A. Abouimrane, I. Belharouak, Y.-K. Sun, *Nano Energy*, 16

(2015) 218.
34. C. Chen, Y. Wen, X. Hu, X. Ji, M. Yan, L. Mai, P. Hu, B. Shan, Y. Huang, *Nat. Commun.*, 6 (2015) 6929.
35. Y. Yeo, J.-W. Jung, K. Park, I.-D. Kim, *Sci. Rep.*, 5 (2015) 13862.
36. S.K. Das, B. Jache, H. Lahon, C.L. Bender, J. Janek, P. Adelhelm, *Chem. Commun.*, 52 (2016) 1428.
37. N. Liu, K. Huo, M.T. McDowell, J. Zhao, Y. Cui, *Sci. Rep.*, 3 (2013) 1919.
38. S. Zhang, M. Zheng, Z. Lin, N. Li, Y. Liu, B. Zhao, H. Pang, J. Cao, P. He, Y. Shi, *J. Mater. Chem. A*, 2 (2014) 15889.
39. J. Ding, H. Wang, Z. Li, K. Cui, D. Karpuzov, X. Tan, A. Kohandehghan, D. Mitlin, *Energy Environ. Sci*., 8 (2015) 941.
40. C. Lv, X. Yang, A. Umar, Y. Xia, Y. Jia, L. Shang, T. Zhang, D. Yang, *J. Mater. Chem. A*, 3 (2015) 22708.
41. N. Sun, H. Liu, B. Xu, *J. Mater. Chem. A*, 3 (2015) 20560.
42. Y.-H. Ding, P. Zhang, H.-M. Ren, Q. Zhuo, Z.-M. Yang, Y. Jiang, *Mater. Res. Bull.*, 46 (2011) 2403.
43. W. Zhang, Y. L. He, M. S. Zhang, Z. Yin, Q. Chen, *J. Phys. D: Appl. Phys*., 33 (2000) 912.
44. C. Kim, S.-H. Park, J.-I. Cho, D.-Y. Lee, T.-J. Park, W.-J. Lee, K.-S. Yang, *J. Raman Spectrosc.*, 35 (2004) 928.
45. F. Yang, Z. Zhang, Y. Han, K. Du, Y. Lai, J. Li, *Electrochim. Acta*, 178 (2015) 871.
46. G. Zou, J. Chen, Y. Zhang, C. Wang, Z. Huang, S. Li, H. Liao, J. Wang, X. Ji, *J. Power Sources*, 325 (2016) 25.
47. S.-D. Xu, Q.-C. Zhuang, L.-L. Tian, Y.-P. Qin, L. Fang, S.-G. Sun, *J. Phys. Chem. C*, 115 (2011) 9210.
48. A. J. Bard, L. R. Faulkner, Electrochemical Methods: Fundamentals and Applications, 2nd ed., John Wiley & Sons Inc., (2001)New York.

© 2017 The Authors. Published by ESG (www.electrochemsci.org). This article is an open access article distributed under the terms and conditions of the Creative Commons Attribution license (http://creativecommons.org/licenses/by/4.0/).